Increases in Life-Safety Risks to Building Occupants from Induced Earthquakes in the Central United States

Taojun Liu,[a), b)] Nicolas Luco,[a)] M.EERI and Abbie B. Liel,[b)] M.EERI

Earthquake occurrence rates in some parts of the central United States have been elevated for a number of years; this increase has been widely attributed to deep wastewater injection associated with oil and gas activities. This induced seismicity has caused damage to buildings and infrastructure and substantial public concern. In March 2016, the U.S. Geological Survey (USGS) published its first earthquake ground motion hazard model that accounts for the elevated seismicity, producing a one-year forecast encompassing both induced and natural earthquakes. To assess the potential impacts of the elevated seismicity on buildings and the public, this paper quantifies forecasted risks of a) building collapse and b) falling of nonstructural building components, by combining the 2016 USGS hazard model with fragility curves for generic modern code-compliant buildings. The assessment shows significant increases in both types of risk compared to that due to non-induced earthquakes alone; the magnitudes of the increases vary from a few times to more than 100 times, depending on location, building period (which is correlated to building height), alternatives for the hazard model, and the type of risk of interest. For exploratory purposes only, we also estimate revised values of the risk-targeted ground motion that are currently used for designing buildings.

INTRODUCTION

The number of earthquakes in the central United States (CUS) has increased dramatically since about 2009 (U.S. Geological Survey, 2016). The earthquakes have mostly occurred in Oklahoma (which has been experiencing thousands of earthquakes above M2.7 per year, with the largest to date of M5.8), but also in Arkansas, Colorado, Kansas, New Mexico, and Texas (Ellsworth, 2013). These elevated earthquake occurrence rates are largely due to deep wastewater disposal associated with oil and gas activities (Ellsworth, 2013; Keranen et al.,

[a)] U.S. Geological Survey, 1711 Illinois St., Golden, CO 80401

2013; Rubinstein et al., 2014; Hough and Page, 2015; Petersen et al., 2015, 2016). While most of the induced earthquakes have been of relatively small magnitude, a number of them have caused damage to homes, masonry buildings, and water distribution systems, as well as minor damage to bridges (Clayton et al. 2016; Taylor et al., 2017; Barba-Sevilla et al., 2018), and many more have been widely felt. The frequent occurrence of such events has led to significant public concerns about the potential damage to or even collapse of buildings that may be caused by ground motions from induced earthquakes, and to increased regulation of wastewater disposal wells in these states.

As a first step in forecasting the ground motion hazard associated with induced earthquakes, the U.S. Geological Survey (USGS) published a report in early 2015, presenting a sensitivity study of alternative probabilistic hazard models that account for the induced seismicity (Petersen et al., 2015). That report aimed to show the effect of various hazard modeling choices on the forecasted ground motion hazard. By combining each alternative induced-seismicity hazard model with the ground motion hazard from natural earthquakes, the report demonstrates that the forecast is sensitive to several key hazard modeling considerations. In addition, the sensitivity analyses indicate that the hazard forecast increases significantly in regions where induced earthquakes have been occurring frequently, regardless of the modeling assumptions made. In March 2016, the USGS published an initial consensus model that developed a ground motion hazard forecast for one year (*i.e.,* 2016) in the central and eastern United States (CEUS) (Petersen et al., 2016). For areas near active induced (or potentially induced) seismicity zones, the ground motion hazard is significantly higher than that due to natural earthquakes alone, although the 2016 model has lower seismic hazard than several of the alternative models considered in the 2015 report. The 2017 and 2018 models are similar to the 2016 model, and fall below some of the alternative models considered in 2015, but above the natural seismicity rate (Petersen et al., 2017; Petersen et al., 2018).

Given the elevated ground motion hazard modeled when induced earthquakes are included in addition to natural earthquakes, we expect higher risk of earthquake-induced damage to buildings. However, the amount of increase in the seismic risk forecast, and its dependence on the type of damage of concern and other variables, is unknown. This study assesses the seismic risk due to both induced and natural seismicity in the CUS, where induced seismicity is most significant. We carry out this risk calculation by combining (i) ground motion hazard curves from the 2016 USGS one-year forecast (Petersen et al., 2016), and (ii) building fragility curves from the *2015 NEHRP (National Earthquake Hazards Reduction Program) Recommended Seismic Provisions for New Buildings and Other Structures* (FEMA, 2015; referred to hereafter as the *2015 NEHRP Provisions*), which is a reference document for U.S. building standards and codes. The hazard curves each quantify an annualized frequency (which can be converted into a probability) of exceeding various ground motion levels at a specified location. As a function of these potential ground motion levels, the building fragility curves each quantify the probability of code-compliant buildings and essential facilities either collapsing or experiencing damage to nonstructural components (*e.g.,* ceiling panels or partition walls) that could fall, potentially endangering life safety and impairing egress. These life-safety risks calculated here are compared with the risk levels accepted in the *2015 NEHRP Provisions* (and the *2016 American Society of Civil Engineers (ASCE) Minimum Design Loads for Buildings and Other Structures*; ASCE, 2016), which consider natural seismicity only. Both ordinary buildings and essential facilities (*e.g.,* hospitals), which have a more demanding design standard, are considered. For exploratory purposes only, we also calculate revised ground motion values for building design that would lower the risks at sites affected by induced and natural seismicity to currently accepted levels.

METHODOLOGY

For a given building and its location, seismic risk can be calculated by combining the ground motion hazard curve for the location and a fragility curve for the building (*e.g.,* McGuire, 2004). In this section of the paper, we first review the risk calculation methodology, and then describe the ground motion hazard and building fragility curves used in our risk calculations.

Calculation of risk

In this study, the mean annual frequency of failure (*i.e.,* the expected number of failures per year) of a performance target (PT, *e.g.,* no collapse), denoted $\lambda[failure\ of\ PT]$, is used to quantify seismic risk. This annual frequency can be calculated through the so-called risk integral (*e.g.,* McGuire, 2004; Luco et al., 2007):

$$\lambda[\text{failure of PT}] = \int_0^\infty \lambda[SA > c] f_{capacity}(c)\,dc, \quad (1)$$

where $f_{capacity}(c)$ represents the derivative of the building fragility curve (and the probability density function of the uncertain building capacity in terms of spectral acceleration, SA), and

$\lambda[SA > c]$ is the ground motion hazard curve (i.e., the mean annual frequency of the ground motion spectral acceleration, SA, exceeding a value corresponding to the building capacity, *c*). Once we obtain the risk through numerical integration of Eq. (1), we convert it to the probability of failure in *t* years via Eq. (2), following the typical assumption that the statistics of such failures can be modeled as a Poisson process. Note that *t* = 50 years is commonly considered by building codes.

$$P[\text{failure of PT in } t \text{ years}] = 1 - \exp(-\lambda[\text{failure of PT}] * t), \qquad (2)$$

Ground motion hazard curves including induced and natural seismicity

The 2014 USGS National Seismic Hazard Model (NSHM) for the United States (Petersen et al., 2014), which is used in building codes (via the aforementioned *2015 NEHRP Provisions*) and other earthquake mitigation applications, purposefully excludes seismicity caused by deep wastewater injection and other human activities. This exclusion is because the NSHM focuses on long-term (*e.g.,* over the next 50 years) forecasts of ground motions from future natural earthquakes, and acknowledges that induced seismicity can change rapidly in time and space due to oil and gas and other activities that can be sensitive to prices and regulations. Nevertheless, in the near-term (*e.g.,* next year), at least, the sharp increase in seismicity in the CUS since about 2009 implies higher ground motion hazard forecasts that should also be modeled.

Focusing on induced-seismicity hazard modeling for the CUS, the 2015 USGS report (Petersen et al., 2015) mentioned earlier in this paper started by demonstrating that the ground motion forecast can be sensitive to several key modeling considerations, such as the maximum magnitude of induced earthquakes. Building upon the 2015 sensitivity analysis, an initial USGS consensus model that forecasts the ground motion hazard for the year 2016 was published (Petersen et al., 2016). In the 2016 model, both induced and natural earthquakes are considered within predefined induced seismicity zones, while earthquakes outside of these zones are treated as natural. Two sub-models, or logic tree branches, of the induced seismicity zones are considered: the “informed” branch considers the possibility that the characteristics of induced earthquakes (such as the maximum magnitude) differ from natural earthquakes, whereas the “adaptive” branch does not differentiate between the two types of earthquakes. Using the same methodology, the USGS published updated one-year forecasts in 2017 and 2018 (Petersen et al., 2017; Petersen et al., 2018) that account for more recent earthquakes.

Ground motion hazard curves from these one-year forecasts are available for a grid of locations covering the conterminous United States and for three different measures of ground motion intensity. In this paper, we focus on the 2016 forecast and the spectral acceleration (SA) measures at 0.2 and 1.0 seconds, which are strongly correlated with the response of low-rise (*e.g.,* 2-story) and mid-rise (*e.g.,* 10-story) buildings. Figure 1 illustrates the hazard curves for SA at 0.2 s for Oklahoma City, Oklahoma ([latitude, longitude] = [35.50°, -97.55°], hereafter "OKC") and Dallas, Texas ([latitude, longitude] = [32.8°, -96.8°], hereafter "DAL"). Also shown in the figure are the hazard curves from the 2014 NSHM (which excludes induced seismicity), those from the alternative induced-seismicity hazard models from the 2015 USGS report, as well as the hazard curves from the 2017 and 2018 one-year forecast models.

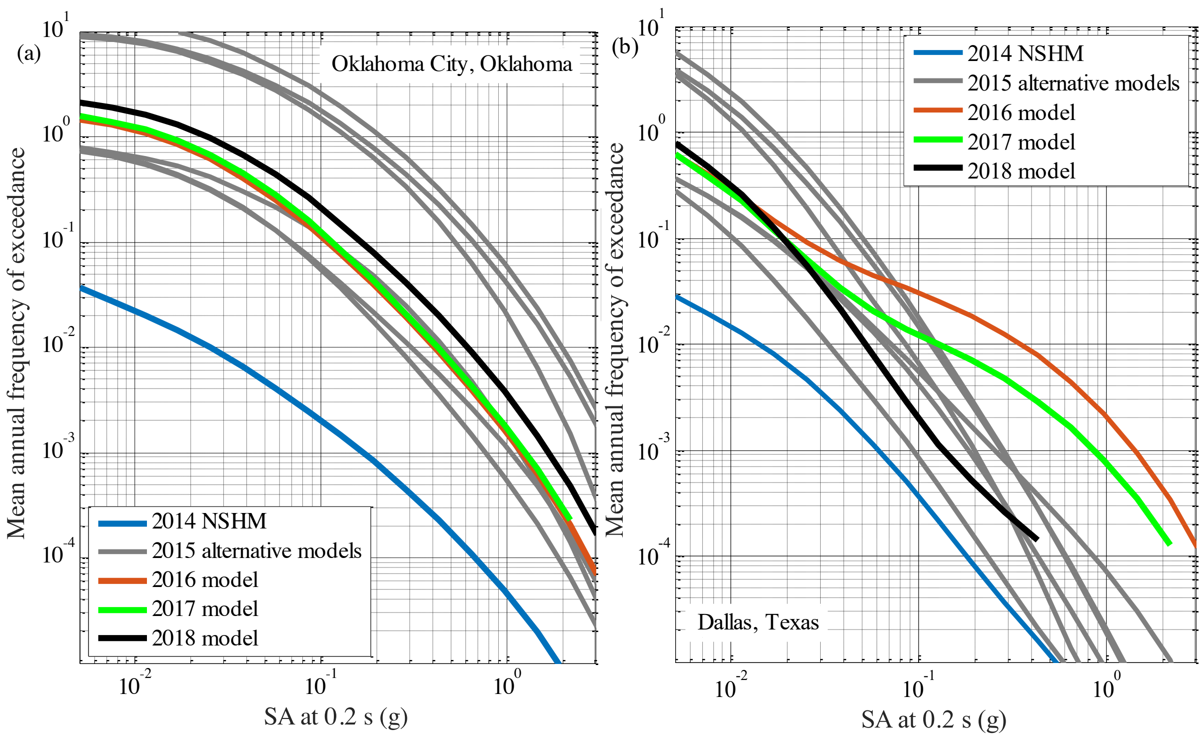

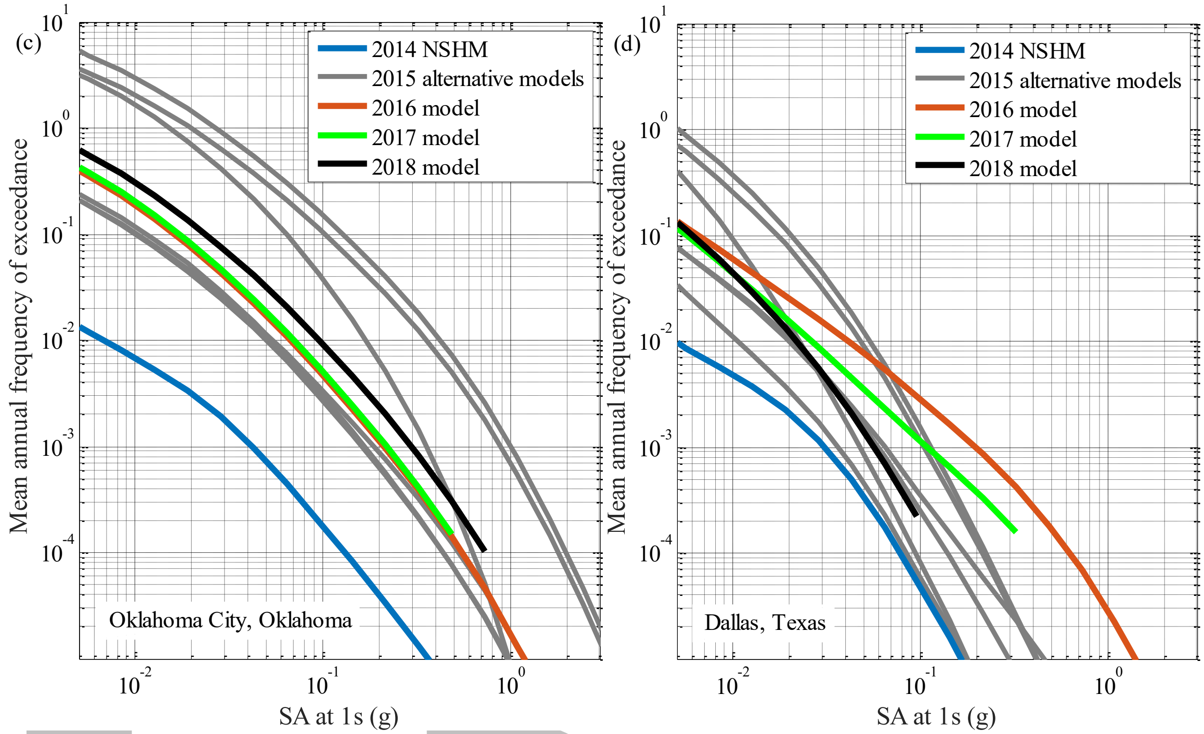

Figure 1. Ground motion hazard curves for spectral acceleration (SA) at 0.2 s from the 2016, 2017and 2018 one-year models, the 2015 alternative models, and the 2014 NSHM for (a) OKC and (b) DAL, and for spectral acceleration (SA) at 1 s for (c) OKC and (d) DAL.

The comparison indicates that including induced seismicity in the 2016, 2017 and 2018 consensus models increases the ground motion hazard forecast over that from the 2014 NSHM, at least at OKC and DAL, by about an order of magnitude. Likewise, Atkinson et al. (2015)'s study of the impact of induced seismicity from hydraulic fracturing operations in Alberta, Canada, observed that the ground motion hazard from induced seismicity can greatly exceed that from natural seismicity. In the CUS, the hazard curves from the 2016 model generally fall between those from the 2015 USGS alternative models, except at DAL, where there is a "bump" in the 2016 hazard curve at moderate to large ground motion (SA) levels. This DAL bump occurs because of a nearby (Irving, Texas) swarm of earthquakes in 2015—potentially induced, but treated as natural in the 2016 model—that were not included in the 2015 alternative models or the 2014 NSHM (see Petersen et al., 2016). The 2017 and 2018 forecasted earthquake hazards are slightly lower in some regions of induced earthquakes (*e.g.,* DAL, as shown in Figure 1), but are still significantly higher than that from the 2014 NSHM. The significant overall increase that results from including induced seismicity is further corroborated by available data discussed in the next subsection.

Comparison of hazard curves with "Did You Feel It?" data

Given the significant increase in ground motion hazard shown in Figure 1, a logical question is: does this hazard forecast reflect the actual ground motions people have experienced? In White et al. (2017), we address this question by comparing the 2016 USGS forecast with the observed and/or felt data from the USGS "Did You Feel It?" (DYFI) system (Wald et al., 2012). DYFI is an online system that collects and archives macroseismic intensity data reported by the public following earthquakes. DYFI has been collecting a vast database of felt intensity and damage effects in the CUS in recent years. The collected intensity data (equivalent to Modified Mercalli Intensity or MMI, Dewey et al., 2000) provide us with an opportunity to compare the estimated hazard with observations, at least for low intensities that are experienced relatively frequently. We compare the model against observed ground motions and damage in 2014-2015. We adopt this approach because the 2016 USGS one-year hazard model is heavily based on the earthquakes of the preceding few years, especially the previous year (*i.e.,* 2015), and the assumption is that past earthquake rates will remain constant over the next year (*i.e.,* 2016).

To compare DYFI data with the hazard, we convert the peak ground acceleration hazard curves from the 2016 hazard model to MMI-based hazard curves, and adjust for site conditions. This facilitates a direct comparison between the hazard model and the hazard curves derived from the DYFI data. Details about the adjustments made to conduct the comparison, and a comprehensive comparison across a broader region are presented in White et al. (2017).

In Figure 2, we show a comparison for OKC between the hazard curves converted from the 2016 USGS one-year hazard model and those derived from the DYFI data. The figure plots both sets of hazard curves within a circular area with radius of 0.05 degree. The figure shows large variability from the DYFI data within a small geographical area due to DYFI sensitivity to population density and other factors (also observed by Mak and Schorlemmer, 2016), as well as the limited (2-year) time horizon of DYFI responses considered. In addition, most of the DYFI responses are in the MMI II-IV range, whereas the hazard model is developed primarily for forecasts at higher ground motion intensities, usually above about MMI IV. Nevertheless, the comparison in Figure 2 indicates good agreement between the 2016 model and the DYFI data in the region of overlap around MMI of IV. Results similar to these are presented in White et al. (2017) for other sites, and many show good agreement, providing some confirmation that the hazard model levels are reasonable.

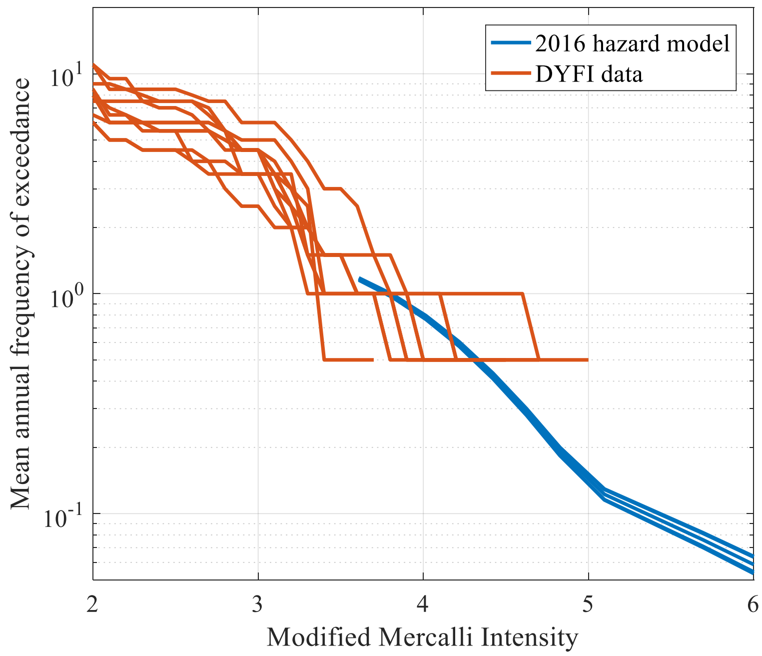

Figure 2. Comparison for OKC between hazard curves converted from the 2016 USGS one-year seismic hazard model and those derived based on the DYFI data from 2014 and 2015. Details of the comparison are provided in White et al. (2017).

Fragility curves defined in the *2015 NEHRP Provisions*

For the fragility curve required for the risk calculation in Eq. (1), we use those defined in the *2015 NEHRP Provisions*. Recall that each fragility curve represents the probability of not satisfying the performance target of interest, as a function of the potential ground motion levels that are represented by the corresponding hazard curve (*e.g.,* see Figure 3(a)). Fragility curves are commonly modeled using lognormal probability distributions. Usually, lognormal distributions are parameterized by a median (50th percentile) and a standard deviation, β. However, they can instead be parameterized by β and the pp^{th} percentile of the distribution, as they are in the *2015 NEHRP Provisions*. For the prevention of structural collapse (*i.e.,* "no collapse") performance target, the *2015 NEHRP Provisions* intend that the probability of collapse of an ordinary-use ("Risk category II") building does not exceed 10%, if subjected to (*i.e.,* "given") a very rare ground motion. That very rare ground motion is the Risk-Targeted Maximum Considered Earthquake (MCE_R) ground motion that is mapped in the *2015 NEHRP Provisions*. This essentially defines the fragility curve by setting its 10th percentile (*i.e.,* pp = 10%) equal to the MCE_R ground motion, as reported in Table 1. Note that because the mapped MCE_R ground motion varies with geographic location, so does the fragility curve. These fragility curves were developed based on analyses of various types of code-conforming buildings (FEMA P-695, 2009), and thus apply in a generic sense to modern buildings complying with code seismic provisions. However, any specific building may have a different fragility, and true capacities to resist ground motion may be higher.

Fragility curves for other performance targets can be defined similarly. Table 1 summarizes a few of the structural (no collapse) and nonstructural (no falling hazard and egress maintained) performance targets for life-safety protection that are defined in the *2015 NEHRP Provisions* (Part 3, Resource Paper 1). Here, we examine the structural performance target for ordinary-use buildings (Risk category II) and for essential facilities such as hospitals (Risk category IV). The nonstructural performance target we examine is for nonessential components such as ceiling panels or partition walls in ordinary-use buildings (see the Table 1 footnote for details; by design, essential components are more likely to meet the performance target). We choose these cases because the collapse fragility curve for ordinary-use buildings (corresponding to *pp* = 10%) was used to determine the mapped MCE_R ground motions in the *2015 NEHRP Provisions*, while the collapse fragility curve for essential facilities and the fragility curve for falling of noncritical nonstructural components represent two extremes, *pp* = 2.5% and *pp* = 25%, respectively. The standard deviation parameter of all the fragility curves is $\beta = 0.6$, consistent with the *2015 NEHRP Provisions*.

Table 1. Structural (no collapse) and nonstructural (no falling hazard and egress maintained) life-safety performance targets examined, and probabilities of not satisfying each performance target under MCE_R ground motions, from the *2015 NEHRP Provisions*.

Performance target	Risk category	Fragility curve percentile, *pp*
No collapse (structural)	II	10%
	IV	2.5%
No falling hazard and egress maintained (nonstructural)	$I_p = 1.0$*	25%

* I_p=1.0 is the importance factor for the design of nonessential nonstructural components of a building, which distinguishes these components from additional design requirements that apply to essential components (I_p = 1.5).

The fragility curves described above are illustrated in Figure 3(a), which shows how *pp* defines the curve. Figure 3(b) plots the derivative of each fragility curve, which is combined with a corresponding ground motion hazard curve to calculate a life-safety risk using Eq. (1). Mainly to set up a discussion later in this paper, note that the peak of the derivative of the fragility curve depends on the performance target. The peak for falling of nonstructural components is close to the MCE_R ground motion level, and therefore this type of life-safety risk is most strongly correlated with the value of the corresponding hazard curve at that ground motion level. The peaks for collapse of ordinary-use buildings and essential facilities are at larger ground motions, indicating that these risks are more correlated with the hazard at larger, less frequently occurring ground motions.

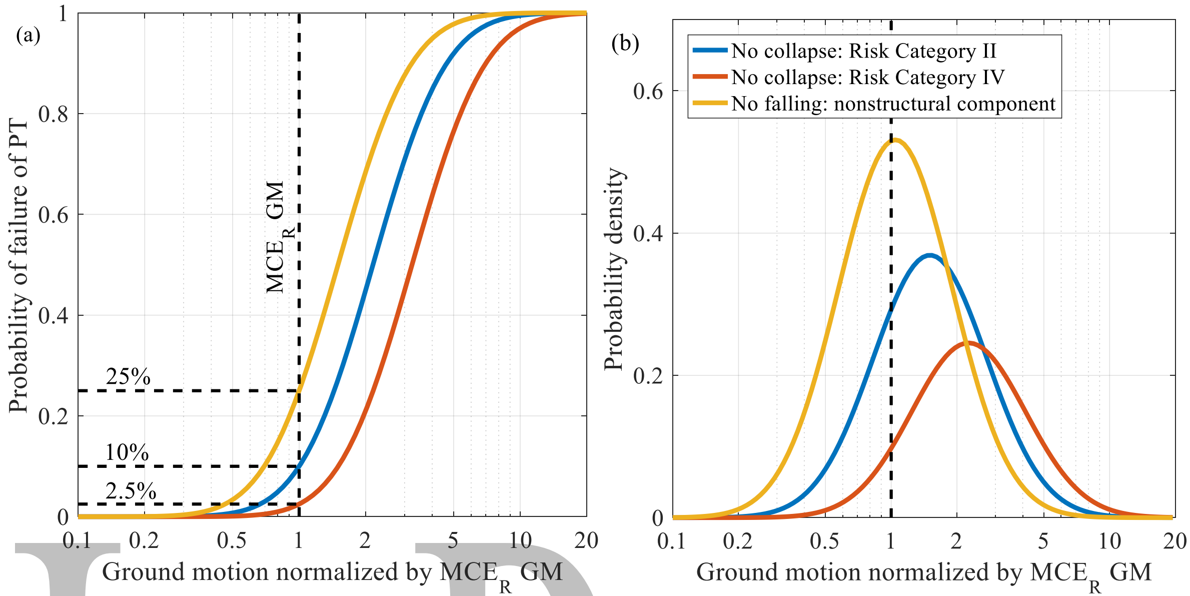

Figure 3. (a) Building fragility curves for the three life-safety performance targets considered in this study and (b) their derivatives used in Eq. (1) to calculate corresponding risks.

RISK ASSESSMENTS

Based on the seismic hazard curves from the 2016 USGS one-year forecast and the fragility curves defined in the *2015 NEHRP Provisions*, we present the calculated risks in this section. We first quantify the collapse risk for ordinary-use buildings, considering buildings of two different periods (*i.e.,* corresponding to two different heights), followed by risk results for the other two performance targets.

Collapse risk for ordinary-use buildings

We present the risk results by calculating the ratio between the collapse risk from the 2016 hazard model, divided by that from the 2014 NSHM; the risk calculated from the 2014 NSHM is implicitly accepted by the *2015 NEHRP Provisions*. (The absolute risks are provided in the electronic supplement Ⓔ). In the following, we focus on the areas where induced seismicity has significantly increased the forecasted hazard, namely Oklahoma, Kansas, and Texas. Figure 4(a) shows the ratio for short-period, 0.2 s, buildings. The figure shows that the collapse risk generally increases, and the most significant increase is near active induced seismicity zones, such as the Oklahoma-Kansas zone, the North Texas zone, and the Venus and Irving zones near Dallas. The increase of collapse risk at the “bull’s-eyes” is more than 100 times.

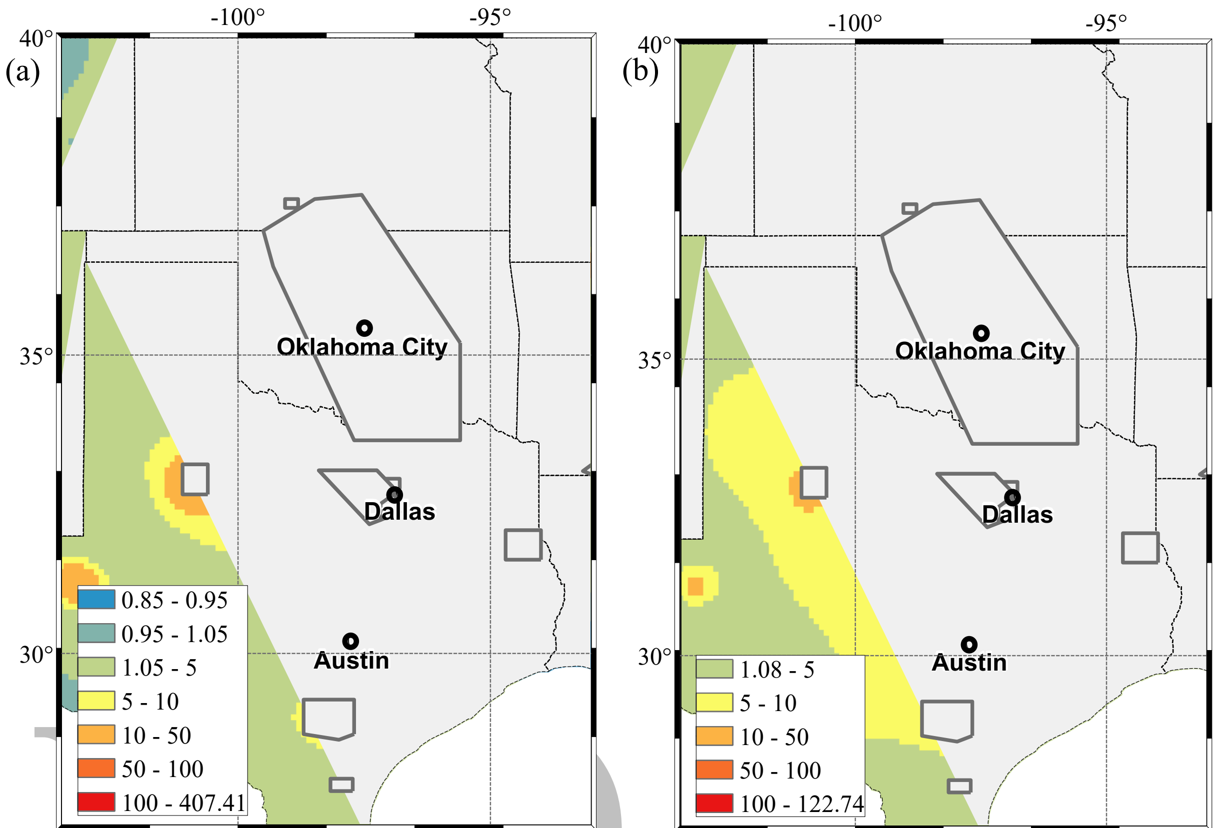

Figure 4. Ratio of the collapse risk for ordinary-use buildings (Risk category II) from the 2016 ground motion hazard model, divided by that implicitly accepted in the *2015 NEHRP Provisions* for buildings of: (a) 0.2 s; (b) 1.0 s. Gray lines indicate induced seismicity zones defined in Petersen et al. (2016).

We note also that for some areas that are far away from active induced seismicity zones, the collapse risk from the 2016 hazard model decreases modestly relative to the 2014 NSHM, as shown in blue in Figure 4(a). This reduction occurs because of the emphasis on the last one to two years of earthquakes in the 2016 hazard model; in 2014 and 2015—the primary basis for the 2016 model—these places experienced less seismicity than that experienced on average over previous years. In other words, the 2016 one-year model depends heavily upon the earthquake rates in the last two years, which may reflect short-term fluctuations in seismicity.

Sensitivity to structural period

The same ratio of risk shown in Figure 4(a) for short-period (0.2 s) ordinary-use buildings is plotted in Figure 4(b) for moderate-period (1.0 s) ordinary-use buildings. We see similar spatial patterns of the risk ratio as we did for short-period buildings. However, the increase of the risk associated with induced seismicity zones is less pronounced for moderate-period buildings compared to short periods. In particular, the largest increase is less, and the area with an increase of more than 100 times is much smaller in Figure 4(b). In contrast, Figure 4(b) shows that the total area affected by moderate-period ground motions is larger. The larger affected area can be attributed to the more gradual energy dissipation or attenuation with respect to distance of moderate-period compared to short-period ground motion content (*e.g.,* Petersen et al., 2014; Atkinson, 2015).

In Figure 5, we report the collapse risk ratio (same ratio shown in Figure 4) for both short- and moderate-period buildings for OKC and DAL. This figure again shows the larger increase in risk at shorter periods compared to longer periods. The figure also shows that the collapse risk ratio is higher for DAL than OKC at short periods. DAL is located on top of a small local induced seismicity zone (Figure 4), so the ground motion hazard is controlled by close-in, smaller magnitude events that increase the risk significantly at short periods. OKC is somewhat farther from the concentration of induced seismicity in Oklahoma and southern Kansas. The collapse risk ratios in DAL and OKC are very similar for moderate-period buildings because the increase in risk tends to be spatially smoother than at short periods.

The reason for the less pronounced increase for moderate-period buildings relates to the maximum magnitudes used in the hazard model. In particular, one of the aforementioned logic tree branches, the "informed branch," predominantly assumes a maximum earthquake magnitude of 6.0 for sources within the induced seismicity zones, which is smaller than the maximum magnitude used for sources outside the zones of induced seismicity (and for all sources in the adaptive branch). The small to moderate magnitude earthquakes that dominate the informed branch produce ground motions with primarily short-period content; this trend is apparent from a comparison of the hazard curves in Figure 1 for 0.2s and 1.0s, which show a greater increase in seismicity for the short-period as compared to moderate-period spectral intensities. Hence, the hazard and risk for moderate to long-period buildings are not increased as much as for short periods, especially in the informed branch of the model (see Figure 5), but also in the combined 2016 model.

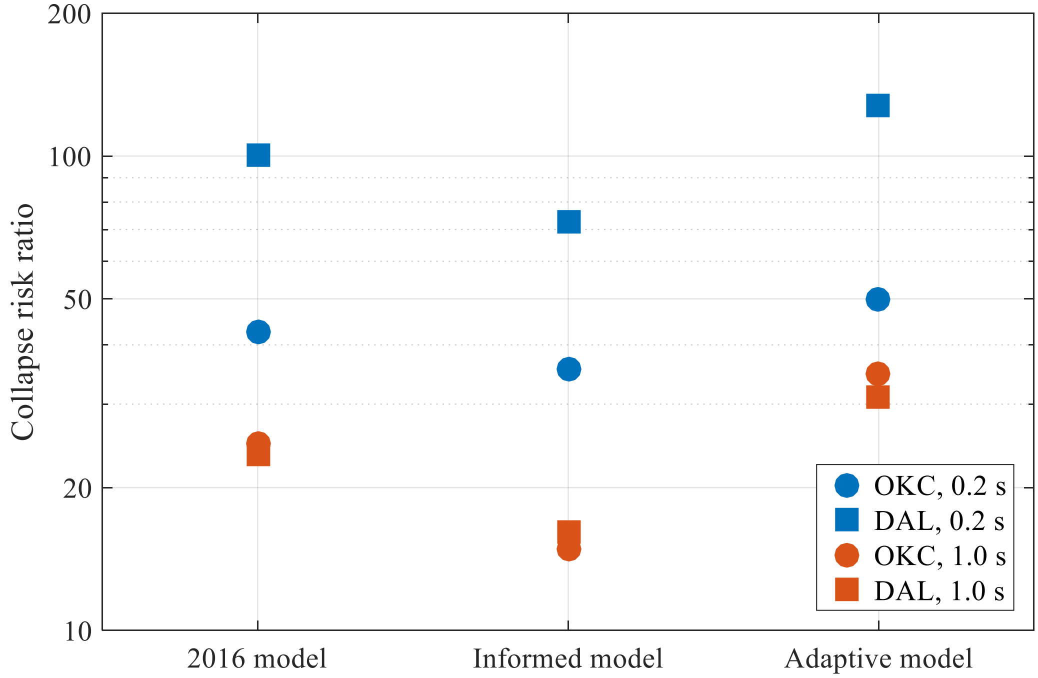

Figure 5. Ratio of the collapse risks for short- (0.2 s) and moderate-period (1.0 s) ordinary-use buildings (Risk category II), due to the 2016 model and its two main sub-models for OKC and DAL, divided by their counterparts accepted in the *2015 NEHRP Provisions*.

Risks for other performance targets

In addition to the collapse risk for ordinary-use buildings, in this section we consider risks for the two other performance targets: no collapse for essential facilities and no falling of nonstructural components. As shown in Figure 3, at a given ground motion level, among the three performance targets considered, the collapse of essential facilities is the least likely to occur (and least acceptable), and the falling of noncritical nonstructural components is the most likely to occur.

Figure 6 maps the ratio between the risk for each of these two performance targets divided by the risk accepted in the *2015 NEHRP Provisions* for the same performance target for short-period buildings. (The absolute risk corresponding to Figure 6, along with the maps for moderate-period buildings are included in the electronic supplement Ⓔ.) At a first glance, Figures 6(a) and 6(b) are similar to Figure 4(a), indicating similar increases in risk for different performance targets. However, at DAL the ratio of increase for the collapse risk for essential facilities is somewhat higher than the ratio for the other performance targets, whereas at OKC it is lower.

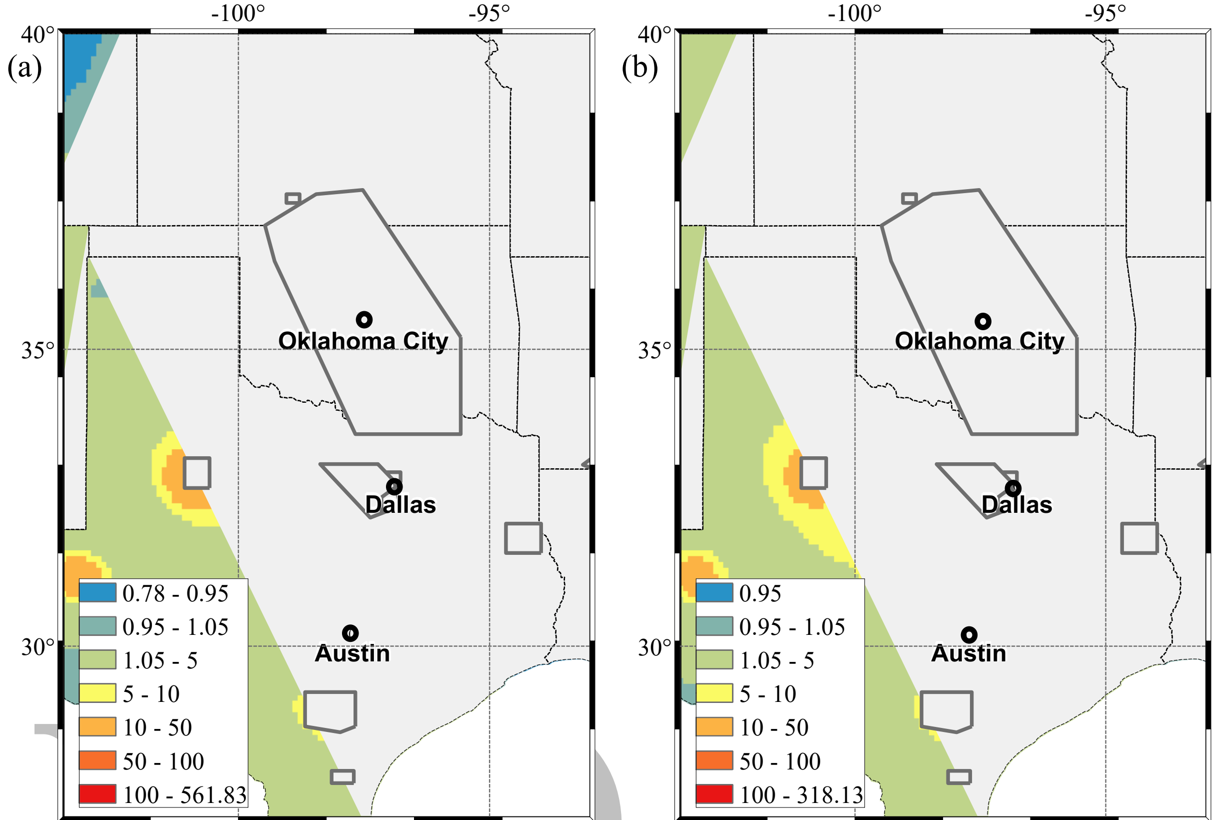

Figure 6. Ratio of (a) collapse risk for short-period (0.2s) essential facilities (Risk category IV) and (b) falling risk for noncritical nonstructural components in short-period buildings due to the 2016 USGS one-year seismic hazard model, divided by their counterparts accepted in the *2015 NEHRP Provisions*.

In Figure 7, we summarize the increase in risk for the different performance targets at OKC and DAL. Note that the results for the collapse risk for ordinary-use Risk Category II buildings (*i.e.,* Collapse risk II on the horizontal axis) are repeated from the results for the 2016 model shown in Figure 5. Figure 7 shows a different trend for risks of the performance targets in OKC compared to DAL. For OKC, the ratio representing the increase in collapse risk for essential facilities is the smallest, compared to the other performance targets, for both short- and moderate-period buildings. For DAL, the increase in risk for essential facilities is the highest of all the performance targets. This is because of the aforementioned bump at the moderate to high ground motion region of the DAL hazard curve (shown in Figure 1(b)), which coincides with the peak of the derivative of the fragility curve for collapse of essential facilities (illustrated in Figure 3(b)), and thereby produces a greater increase in the estimated risk. These observations are consistent with the general trends in Figure 6, in that DAL is located on top of a small local induced seismicity zone, whereas OKC is close to the large zone in Oklahoma and southern Kansas (but farther away from the nearest source than DAL).

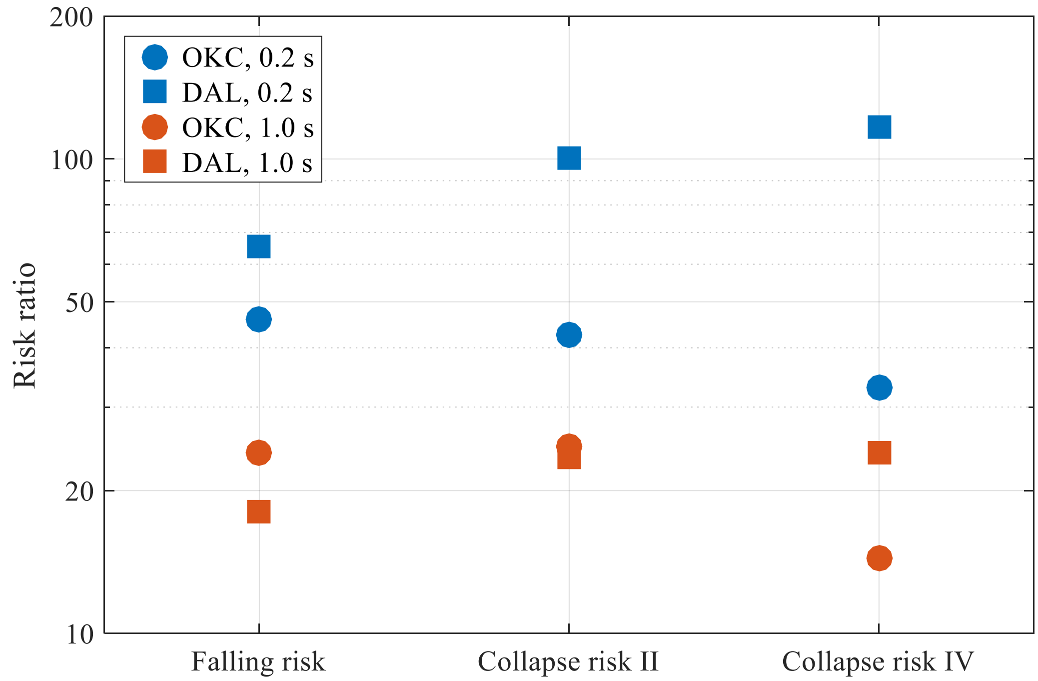

Figure 7. Ratio of risks computed using the 2016 model divided by their counterparts accepted in the *2015 NEHRP Provisions*, for OKC and DAL for short- (0.2 s) and moderate-period (1.0 s) buildings. Three performance targets are considered: no collapse for ordinary-use buildings (Collapse risk II) and essential facilities (Collapse risk IV), and no falling of noncritical nonstructural components.

Expected risks based on the 2017 and 2018 USGS one-year hazard forecasts

As demonstrated in Figure 1, the 2017 and 2018 USGS one-year hazard forecast is similar to the 2016 model at OKC but somewhat lower at DAL, due to a lower rate of earthquakes there in 2016-2017 compared to 2014-2015. Even at DAL, though, the hazard remains significantly elevated over that from non-induced earthquakes alone (*i.e.,* the 2014 USGS model). As a result, from the 2017 and 2018 models, we can still expect an elevated risk compared to the levels accepted in the *2015 NEHRP Provisions,* for all the building periods and performance targets of interest. Despite a steady decline in seismicity since 2015, the 2018 model ground motions remain significantly elevated from the natural seismicity level (Figure 1). For Dallas in particular, there has been some reduction in forecasted ground motions which would, accordingly, lower the risks calculated here. Nevertheless, these risks remain higher than anticipated in the *2015 NEHRP Provisions.*

INVESTIGATION OF RISK-TARGETED DESIGN GROUND MOTIONS

One method for responding to an increase in seismic risk is to design buildings for a higher ground motion level to mitigate the risk. At this time, building code committees in the U.S. are unlikely to adopt this approach, due to the transient and potentially controllable nature of induced earthquakes that is at odds with the roughly 50-year lifespan of buildings. Even so, we provide an investigation of the design ground motions that could counteract the increased risk, for exploratory purposes. Here, we adopt the concept of risk-targeted ground motions to calculate the ground motion level for which one could achieve the same risk level accepted in the *2015 NEHRP Provisions*. The risk-targeted ground motions in the *2015 NEHRP Provisions* target 1% in 50 years collapse risk ($\lambda[collapse] = 2.01\times10^{-4}$ collapses per year) for ordinary buildings, based on the same 'no collapse' fragility for ordinary-use buildings defined previously. However, Luco et al. (2017) and Liu et al. (2017) have shown that the collapse risk for ordinary-use buildings is as much as 10 times higher than this target (*i.e.,* $\lambda[collapse] = 2.01\times10^{-3}$ per year) in some places in California, due to the use of deterministic ground motion caps in the definition of design values, especially close to active faults. Since this higher risk is (implicitly) accepted in some parts of California, we use it as a second target for the risk-targeted ground motions under both induced and natural earthquake hazard.

In this section, we calculate revised Risk Targeted Maximum Considered Earthquake ground motions for different sites, $RTGM_{2016}$, that, if used in design, would achieve the risk targets of 1% in 50-year collapse risk ($\lambda[collapse] = 2.01\times10^{-4}$ per year) or the higher ~10% in 50-year collapse risk level ($\lambda[collapse] = 2.01\times10^{-3}$ per year). Conservatively, we define MCE_{R2016} ground motion as the larger of $RTGM_{2016}$ and the MCE_R ground motions from the *2015 NEHRP provisions*. Based on this definition, the MCE_{R2016} ground motions would provide similar levels of protection for regions affected by natural earthquakes alone and those near active induced seismicity zones.

Figure 8 maps the ratio between MCE_{R2016} and *2015 NEHRP Provisions* MCE_R ground motions for short-period buildings. For Figure 8(a), MCE_{R2016} ground motions are calculated based on $RTGM_{2016}$ targeting 1% in 50-year collapse risk; for Figure 8(b), $RTGM_{2016}$ targets 10% in 50-year collapse risk. For sites where natural earthquakes govern the hazard, there is no change between MCE_{R2016} and MCE_R ground motions. In Figure 8(a), there are large increases (up to 20 times) reflected in MCE_{R2016} to counteract the induced earthquake hazard. There is no change for most areas in Figure 8(b), because the higher risk target moderates the need to increase the design ground motion level, even where there is some induced activity. However, for sites near active induced seismicity zones, there is an increase between MCE_R and MCE_{R2016} by a factor of about 11. The ratios in Figure 8(b) correspond to absolute differences from MCE_R to MCE_{R2016} of 0 g to 1.35 g for short periods (0.2s). Not surprisingly, the largest increase to the MCE_R ground motion levels occurs near the Oklahoma-Kansas zone (although the precise location of the largest increase depends upon whether it is quantified as a ratio or as a difference in absolute terms). Maps showing the changes between MCE_{R2016} and *2015 NEHRP Provisions* MCE_R ground motions in terms of their difference, as well as comparison of MCE_{R2016} and *2015 NEHRP Provisions* MCE_R ground motions maps for moderate-period buildings are included in the electronic supplement Ⓔ.

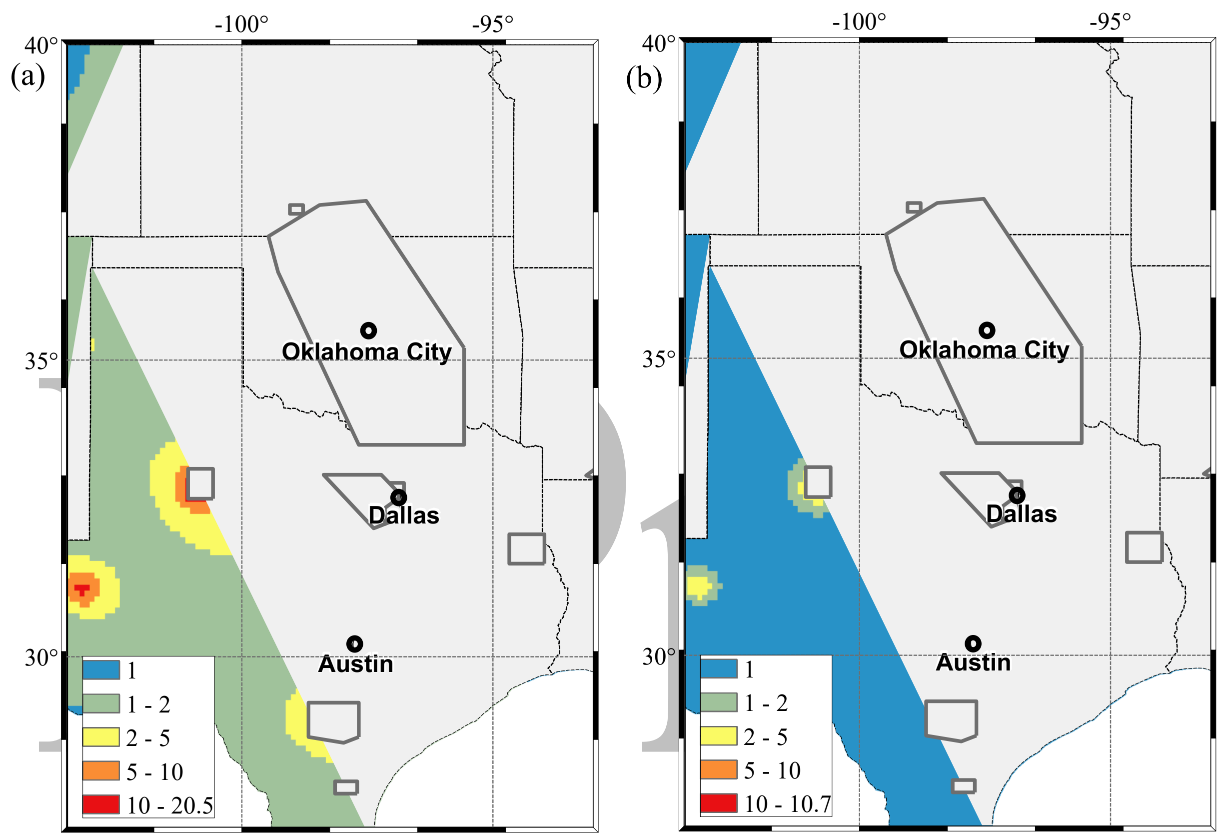

Figure 8. Ratio between short-period (0.2 s) MCE_{R2016} ground motions and the MCE_R ground motions from the *2015 NEHRP Provisions*: (a) MCE_{R2016} based on $RTGM_{2016}$ targeting 1% in 50-year collapse risk and (b) MCE_{R2016} based on $RTGM_{2016}$ targeting ~10% in 50-year collapse risk.

In U.S. building codes and standards, *e.g.,* the *2015 NEHRP Provisions* as adopted by *ASCE 7* (2016), key design provisions, including the required lateral strength, drift limits, and detailing specifications, depend on Seismic Design Category (SDC). These SDCs range from ‘A’ to ‘F,’ with more stringent design and detailing requirements applying to the later letters. A site’s SDC depends on the building’s risk category and the amplitude of design ground motions at the site (*i.e.,* MCE_R modified based on site condition). To examine how changes in MCE_{R2016} might influence SDC assignment in the CUS, we compare the SDC with or without the increase in design ground motions for ordinary-use buildings (Risk category II); thus, we compare the SDC based on MCE_{R2016} to the SDC based on MCE_R. Assuming site class D, SDC

B is obtained for both OKC and DAL if the design motions based on natural seismicity in the current building codes are used (*i.e.,* MCE_R). Figure 9(a) maps the increase of SDC if MCE_{R2016} ground motions target the 1% in 50-year collapse risk. The SDC for the majority of the area increases by one category, and for some locations it increases by up to three categories. In particular, SDC would increase from B to D for both OKC and DAL. If MCE_{R2016} ground motions are calculated based on the higher risk target (*i.e.,* 10% in 50-year collapse risk), the increase of SDC is shown in Figure 9(b). In Figure 9(b), the SDC increases only in the area where the design ground motions change significantly; the largest increase is two categories (*i.e.,* from SDC B to D) for some sites in Oklahoma, Kansas and Texas. The locations where the SDC increases coincide with the largest differences (in absolute terms, rather than a ratio) between MCE_{R2016} and MCE_R ground motions (Figure 8).

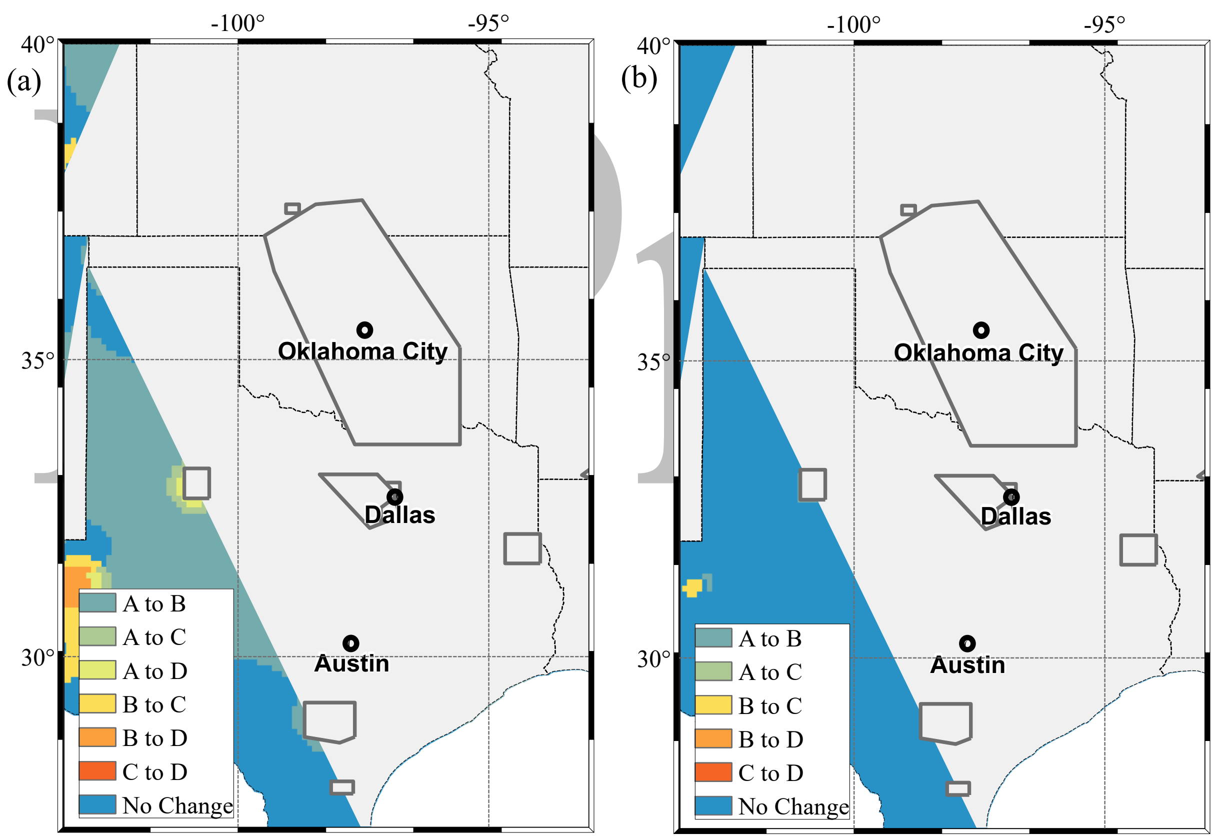

Figure 9. Increase of Seismic Design Category: (a) considering MCE_{R2016} ground motions targeting 1% in 50-year collapse risk; (b) considering MCE_{R2016} ground motions targeting 10% in 50-year collapse risk.

CONCLUSIONS

This study presents a quantitative assessment of life-safety risks in buildings accounting for both induced and natural seismicity in the CUS. These life-safety risk calculations are based on the USGS 2016 one-year seismic hazard model and the fragility curves defined in the *2015 NEHRP Provisions*, considering risks from building collapse and falling hazards.

The findings show that the life-safety risks to building occupants for modern buildings in regions close to active induced seismicity zones can be significantly higher than the levels accepted in the *2015 NEHRP Provisions*, which only considers natural seismicity. Depending on the location, fundamental period of vibration of the building, and the performance target, the increase in risk varies from a few times to more than 100 times. In particular, the risks for short-period buildings are increased more significantly by induced earthquakes than the risks for moderate-period buildings. Three building performance targets associated with endangering life safety were considered, namely collapse of ordinary-use (Risk Category II) buildings, collapse of essential facilities like hospitals (Risk Category IV), and falling hazards from nonstructural components. At a given site, the relative increase in risk when induced earthquakes are considered is of the same order of magnitude for all three performance targets. However, characteristics of the hazard at the site affect which performance target sees the largest relative increase. These findings are based on the 2016 model, but similar results would be expected for the 2017 and 2018 one-year models, which also indicated significantly elevated hazard relative to the natural seismicity level. It follows that collapse risk for older buildings, with greater fragility, would also be increased, although it is not shown here.

In addition to quantifying the increases in risk, we explored increases in building code ground motions that could maintain the risk levels targeted by the *2015 NEHRP Provisions*, as well as the levels implicitly accepted by the *2015 NEHRP Provisions,* while considering the 2016 one-year hazard model. These increases are provided to inform users who are interested in quantifying the design level necessary to mitigate the increased risk. However, the increased design values from the 2016 one-year hazard forecast are likely not appropriate for building code adoption because building codes are intended for design of buildings with roughly 50-year lifespans, whereas the 2016 hazard model is only for one specific year. Even so, the increase in Seismic Design Category that we also explored could be considered for building codes in regions close to active induced seismicity zones.

ACKNOWLEDGMENTS

The authors acknowledge the financial support from the National Science Foundation (NSF, Award Number: 1520846). In addition, T.J. Liu would like to acknowledge the postdoctoral fellowship awarded by the Natural Sciences and Engineering Research Council of Canada. We thank Isabel White for her help in developing Figure 2, and appreciate reviews by Robert Williams of the U.S. Geological Survey and two anonymous reviewers.

REFERENCES

American Society of Civil Engineers (ASCE), 2016. *Minimum Design Loads for Buildings and Other Structures, ASCE/SEI 7-16*, Reston, VA.

Atkinson, G.M., 2015. Ground-motion prediction equation for small-to-moderate events at short hypocentral distances, with application to induced-seismicity hazards, *Bulletin of the Seismological Society of America*, **105**(2A), 981-992.

Atkinson, G.M., Ghofrani, H. and Assatourians, K., 2015. Impact of induced seismicity on the evaluation of seismic hazard: Some preliminary considerations, *Seismological Research Letters*, **86**(3), 1009-1021.

Barba-Sevilla, M., Baird, B.W, Liel, A.B. and Tiampo, K.F., 2018. Hazard implications of the 2016 Mw 5.0 Cushing, OK earthquake from a joint analysis of damage and InSAR data, 2018. *Remote Sensing,* **10**(11), 1715.

Clayton, P., Zalachoris, G., Rathje, E., Bheemasetti, T., Caballero, S., Yu, X., and Bennett, S., 2017. “The Geotechnical Aspects of the September 3, 2016 M5.8 Pawnee, Oklahoma Earthquake.” GEER Reconnaissance Reports.

Der Kiureghian, A., 2005. Non-ergodicity and PEER's framework formula, *Earthquake Engineering & Structural Dynamics*, **34**(13), 1643-1652.

Dewey, J., Wald, D., and Dengler, L., 2000. Relating conventional USGS modified Mercalli intensities to intensities assigned with data collected via the Internet, *Seismological Research Letters*, **71**(2), 264.

Ellsworth, W.L., 2013. Injection-induced earthquakes, *Science* **341**(6142), 1225942.

Federal Emergency Management Agency (FEMA), 2009. *Quantification of seismic performance factors*.

Federal Emergency Management Agency (FEMA), 2015. *NEHRP Recommended Seismic Provisions for New Buildings and Other Structures*.

Hough, S.E., and Page, M., 2015. A century of induced earthquakes in Oklahoma? *Bulletin of the Seismological Society of America* **105**(6), 2863-2870.

Keranen, K.M., Savage, H.M., Abers, G.A., and Cochran, E.S., 2013. Potentially induced earthquakes in Oklahoma, USA: Links between wastewater injection and the 2011 Mw 5.7 earthquake sequence, *Geology*, **41**(6), 699-702.

Liu, T.J., Luco, N., Liel, A.B., and Hoover, S.M., 2017. Building Collapse and Life Endangerment Risks from Induced Seismicity in the Central and Eastern United States, Paper No. 3946, in *Proceedings*, *16th World Conference on Earthquake Engineering*, 9-13 January 2017, Santiago, Chile.

Luco, N., Ellingwood, B.R., Hamburger, R.O., Hooper, J.D., Kimball, J.K., and Kircher, C.A., 2007. Risk-targeted versus current seismic design maps for the conterminous United States, in *Proceedings*, *Structural Engineers Association of California Convention*, 26-29 September 2007, Squaw Creek, California.

Luco, N., Liu, T.J., and Rukstales, K., 2017. A risk-targeted alternative to deterministic capping of maximum considered earthquake ground motion maps, Paper No. 4538, in *Proceedings*, *16th World Conference on Earthquake Engineering*, 9-13 January 2017, Santiago, Chile.

Mak, S. and Schorlemmer, D., 2016. What Makes People Respond to "Did You Feel It?"?, *Seismological Research Letters*, **87**(1), 119-131.

McGuire, R.K., 2004. *Seismic hazard and risk analysis*. Earthquake engineering research institute, 221 pp.

Petersen, M.D., Moschetti, M.P., Powers, P.M., Mueller, C.S., Haller, K.M., Frankel, A.D., Zeng, Y., Rezaeian, S., Harmsen, S.C., Boyd, O.S., Field, N., Chen, R., Rukstales, K.S., Luco, N., Wheeler, R.L., Williams, R.A., and Olsen, A.H., 2014. *Documentation for the 2014 update of the United States national seismic hazard maps, Open-File Report 2014-1091*. U.S. Geological Survey, Golden, CO.

Petersen, M.D., Mueller, C.S., Moschetti, M.P., Hoover, S.M., Rubinstein, J.L., Llenos, A.L., Michael, A.J., Ellsworth, W.L., McGarr, A.F., Holland, A.A., and Anderson, J.G., 2015. *Incorporating induced seismicity in the 2014 United States National Seismic Hazard Model: results of the 2014 workshop and sensitivity studies, Open-File Report 2015-1070*, U.S. Geological Survey, Golden, CO.

Petersen, M.D., Mueller, C.S., Moschetti, M.P., Hoover, S.M., Llenos, A.L., Ellsworth, W.L., Michael, A.J., Rubinstein, J.L., McGarr, A.F., and Rukstales, K.S., 2016. *One-year seismic hazard forecast for the central and eastern United States from induced and natural earthquakes, Open-File Report 2016-1035*, U.S. Geological Survey, Golden, CO.

Petersen, M.D., Mueller, C.S., Moschetti, M.P., Hoover, S.M., Shumway, A.M., McNamara, D.E., Williams, R.A., Llenos, A.L., Ellsworth, W.L., Michael, A.J., Rubinstein, J.L., McGarr, A.F., and

Rukstales, K.S., 2017. 2017 One-Year Seismic-Hazard Forecast for the Central and Eastern United States from Induced and Natural Earthquakes, *Seismological Research Letters*, **88**(3), 772-783.

Petersen, M.D., Mueller, C.S., Moschetti, M.P., Hoover, S.M., Rukstales, K.S., McNamara, D.E., Williams, R.A., Shumway, A.M., Power, P.M., Earle, P.S., Llenos, A.L., Michael, A.J., Rubinstein, Norbeck, J.H., Cochran, E.S. 2018. 2018 One-Year Seismic-Hazard Forecast for the Central and Eastern United States from Induced and Natural Earthquakes, *Seismological Research Letters*, **89**(3), 1049-1061.

Rubinstein, J.L., Ellsworth, W.L., McGarr, A., and Benz, H.M., 2014. The 2001–present induced earthquake sequence in the Raton Basin of northern New Mexico and southern Colorado, *Bulletin of the Seismological Society of America* **104**(5), 2162-2181.

Taylor, J.; Çelebi, M.; Greer, A.; Jampole, E.; Masroor, A.; Melton, S.; Norton, D.; Paul, N.;Wilson, E.; Xiao, Y., 2017. EERI Earthquake Reconnaissance Team Report: M5.0 Cushing, Oklahoma, USA Earthquake on November 7, 2016..

U.S. Geological Survey, 2016. http://earthquake.usgs.gov/research/induced/, last accessed June 2016.

Wald, D.J., Quitoriano, V., Worden, C.B., Hopper, M., and Dewey, J.W., 2011. USGS "Did you feel it?" internet-based macroseismic intensity maps, *Annals of Geophysics*, **54**(6), 688-707.

White I., Liu, T.J., Luco, N., and Liel, A.B., 2017. Considerations in comparing the U.S. Geological Survey one-year induced-seismicity hazard models with "Did You Feel It?" and instrumental data, *Seismological Research Letters*, **89**(1), 127-137.